



Study of Different Properties of Graphene Oxide (GO) and Reduced Graphene Oxide (rGO) †

Prateek Viprya ¹, Dhruva Kumar ^{1,*}  and Suhas Kowshik ² 

¹ Department of Mechanical Engineering, Sikkim Manipal Institute of Technology, Sikkim Manipal University, Majitar 737132, Sikkim, India; prateekviprya1928@gmail.com

² Department of Mechanical and Industrial Engineering, Manipal Institute of Technology, Manipal Academy of Higher Education, Manipal 576104, Karnataka, India; suhas.kowshik@manipal.edu

* Correspondence: dhruva.ju@gmail.com

† Presented at the International Conference on Recent Advances in Science and Engineering, Dubai, United Arab Emirates, 4–5 October 2023.

Abstract: Graphene oxide (GO) and reduced graphene oxide (rGO) are well known for their exceptional characteristics in a variety of applications. Reduced graphene oxide differs from graphene oxide in terms of morphological aspects, quality, functionalized groups, and crystallinities. Several attempts to synthesize GO and rGO have been documented in studies. The paper discussed the numerous ways to synthesize GO and rGO, and a literature review revealed that Hummers' technique stands out as the most commonly used. Graphite is mixed with potassium permanganate, sodium nitrate, and strong sulfuric acid to make GO. Notably, Hummers' technique has the advantage of faster synthesis and higher GO quality. The paper discusses several investigations, including the morphological and structural characteristics, chemical bonding information, and mechanical properties of GO and rGO. Scanning Electron Microscopy (SEM), Atomic Force Microscopy (AFM), X-ray Diffraction (XRD), Fourier Transform Infrared Spectroscopy (FTIR), and the Vickers Hardness Tester are generally used to study these characteristics. The FTIR analysis revealed that the most common peaks in both GO and rGO were found to be associated with the O-H, C=O, C-OH, and C-O functional groups. XRD examination, on the other hand, revealed a diffraction peak at $2\theta = 10.2^\circ$, indicating oxidized graphite in the case of GO, as well as a graphitic peak at $2\theta = 26.3^\circ$, indicating graphitic graphite. Furthermore, the addition of GO and rGO into ceramics or polymers was discovered to cause significant changes in their mechanical characteristics, such as tensile strength, Young's modulus, and others. This demonstrates the revolutionary potential of graphene in improving the performance of composite materials.

Keywords: graphene oxide (GO); synthesis; SEM; FTIR; XRD



Citation: Viprya, P.; Kumar, D.; Kowshik, S. Study of Different Properties of Graphene Oxide (GO) and Reduced Graphene Oxide (rGO). *Eng. Proc.* **2023**, *59*, 84. <https://doi.org/10.3390/engproc2023059084>

Academic Editors: Nithesh Naik, Rajiv Selvam, Pavan Hiremath, Suhas Kowshik CS and Ritesh Ramakrishna Bhat

Published: 20 December 2023



Copyright: © 2023 by the authors. Licensee MDPI, Basel, Switzerland. This article is an open access article distributed under the terms and conditions of the Creative Commons Attribution (CC BY) license (<https://creativecommons.org/licenses/by/4.0/>).

1. Introduction

Graphene oxide (GO) is a material that attracts considerable attention in the scientific community due to its unique physical and chemical characteristics. Its properties can be tuned by varying the degree of oxidation, the size and shape of the flakes, and the chemical functionalization, which makes it a versatile material with great potential for various applications. Graphene-based material has excellent mechanical [1], thermal [2,3], and electrical [1,4] properties, making it a potential candidate for use in energy storage [5], biosensors [5], biomedical engineering [6], hydrogen storage, displays, and solar cells [7,8]. GO has potential application in environmental remediation due to its ability to absorb various pollutants, such as heavy metals and organic contaminants, making it a promising material for water purification and desalination [9].

The synthesis of graphene oxide (GO) was first carried out by Brodie [10] and modified by Hummers [11]. The molecular structure of GO, according to these authors, is that of a

carbon compound with oxygen functional groups bonded to carbon atoms in the hexagonal plane [12]. Graphene has a flexible structural shape, remarkable mechanical strength, and zero bandgaps [13,14].

2. Method for Synthesis of GO and rGO

Synthesis of GO and rGO

Reduced GO is obtained by the removal of oxygen from the GO structure. GO is produced via methods such as Hummers' (oxidation with sulfuric acid, potassium permanganate) and Brodie's (nitric acid oxidation) [14]. By using sulfuric acid to raise the mixture's acidity and multiple aliquots of solid KClO_3 throughout the reaction in 1898, Staudenmaier improved Brodie's process. This method, known as Staudenmaier's method, produces hazardous ClO_2 gas, which breaks down in the air and causes explosions [15].

Alghyamah et al. (2022) created rGO by reducing GO in situ inside the PEO matrix while employing L (+) Ascorbic acid as a green reductant [16]. Chaiyakun et al. (2012) synthesized the GO nanosheet using Hummers' method by mixing natural graphite powder and sodium nitrate with sulfuric acid and stirring with potassium permanganate [17]. Ban et al. (2012) used strong oxidizing agents, stirred with a magnetic stirrer, added potassium permanganate, and stirred for three days to obtain GO [18]. Zhou et al. (2013) employed Hummers' method, involving graphite, H_2SO_4 , NaNO_3 , KMnO_4 , heat, water, and centrifugation, to produce graphene oxide (GO) powder [19]. Lavin-Lopez et al. (2017) created rGO by combining thermal and chemical processes, employing hydrazine and ascorbic acid as reducing agents. The products' names were Hydrazine Multiphase Reduced Graphene Oxide (HMP-rGO) and Ascorbic acid Multiphase Reduced Graphene Oxide (AMP-rGO) [20]. Graphite modified via Hummers' method; mixed with KMnO_4 , H_2SO_4 ; water, H_2O_2 added for brown GO solution. Filtered, washed, and thermally reduced to rGO at 750 °C with argon [21].

3. Characterization

3.1. Scanning Electron Microscope (SEM)

Scanning electron microscopy (SEM) determines surface morphology and the number of graphene layers. This is achieved by focusing a beam of energetic electrons onto the sample. The morphological characteristics of GO and rGO can be explained using SEM [22]. Handayani et al. (2019) analyzed GO samples using SEM at 10k, 25k, and 40k magnifications, revealing thicker edges due to oxygen functional groups. EDS (Energy Dispersive X-ray Spectroscopy) confirmed carbon and oxygen composition (shown in Figure 1) [1]. Analysis of graphite, GO, and rGO reveals platelet-like crystals, wrinkled flakes, and disordered crumpled sheets, respectively, through SEM (Figure 2) [23,24]. Cheng-an et al. (2017) used SEM to observe the lamella structures of GO composite films. Increased GO concentration led to organized and stratified deposition, with well-organized GO stacks in 50% GO composite film [25]. During a comparison between graphite powder and rGO using SEM at 10k magnification, lemon juice was found to be effective in reducing rGO thickness from 26.4–29.3 nm [26]. Long-term ball milling results in shrinking ZnO particle size and damaged hexagonal crystals. In the hybrid nanocomposite, ZnO nanoparticles adhere to the rGO surface [27]. A study of the surface morphology of pristine GO foils revealed smooth surface images at low and high magnification, with an average roughness profile of 0.6 μm at a sub-micrometric scale [28]. Analyzing fractured surfaces in composites. Plain cement showed cracks passing through hydration products, while GO-cement displayed crack deflection, impeding crack propagation on increasing load [29]. Salinization makes GO shorter and smoother [30]. An SEM image of rGO that had been dried at 80 °C for a day shows a folded shape typical of a few-layer rGO (thickness 10 nm), huge dimensions (>100 nm), and re-stacked layers [31]. While analyzing GO papers through SEM, thicker papers showed increased roughness due to flake stacking and blockage of the flow path, resulting in wrinkles and surface roughness [32]. SEM reveals unevenly scattered rGO on fibers and displays cycle-dependent accumulation, color change, and dispersed rGO [33].

While GO nanosheets with characteristic folds and wrinkles show that graphite oxide exfoliation successfully produced 2D nanosheets [34].

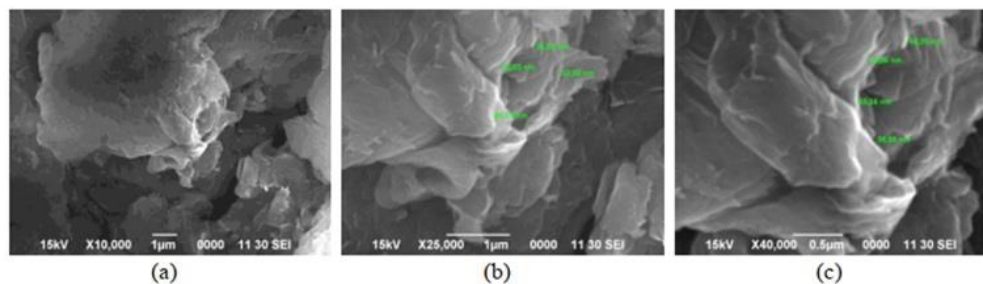


Figure 1. Examination of GO sample using SEM: (a) 10k magnification; (b) 25k magnification; (c) 40k magnification.

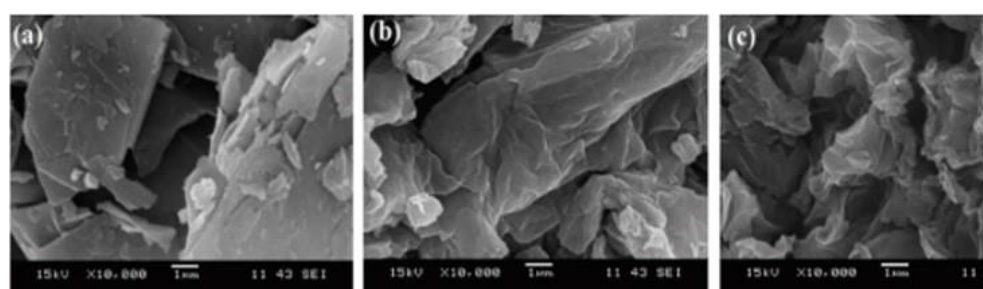


Figure 2. 10,000 \times magnification SEM image of (a) graphite; (b) GO; (c) rGO.

3.2. FTIR Spectroscopy

FTIR (Fourier transform infrared) is the most common form of infrared spectroscopy. FTIR spectra analysis was performed to investigate the structure and functional groups of the materials [35]. FTIR analysis of rGO showed O-H ($\sim 3464\text{ cm}^{-1}$), C=O ($\sim 1639\text{ cm}^{-1}$), C-OH ($\sim 1288\text{ cm}^{-1}$), C-O ($\sim 1003\text{ cm}^{-1}$) peaks, with weak C=C ($\sim 1493\text{ cm}^{-1}$), indicating GO oxidation. Reduction weakens/eliminates peaks over time [1,36]. Peaks at 1081 cm^{-1} (C-O bond), $1630\text{--}1650\text{ cm}^{-1}$ (C=C bond), and a broad peak at $2885\text{--}3715\text{ cm}^{-1}$ (O-H stretch), confirm GO's absorbent nature (Figure 3) [17,18]. The peak at 2135 cm^{-1} identifies the Si-H group [21]. The broad peak from 2885 cm^{-1} to 3715 cm^{-1} indicated absorbed water, supporting GO's high absorbency and gel-like behavior [37,38]. FTIR spectroscopy assesses oxygen-functional group integration in carbon lattice, identifying key modes such as C-O, C-OH, O-H vibrations, C=O, and C-H stretching vibrations [39]. Peaks at 1726 cm^{-1} , 1115 cm^{-1} , and 1074 cm^{-1} confirm graphite oxidation and hydrophilicity [40]. GO exhibits C-OH (3407 cm^{-1}) and -COOH (1730 cm^{-1}) groups [41]. FTIR analysis reveals GO has C-O, C-O-C, C-OH, C=O, and O-H peaks. rGO reduced (1160 cm^{-1} , 1550 cm^{-1}). SRGO sulfonated (1034 cm^{-1} , 1160 cm^{-1}). The results suggest the successful sulfonation of rGO, enhancing solubility, stability, and dispersibility in polar solvents (Figure 3) [42]. GO composite exhibits MgO-water interaction, decreased GO peaks, hydroxyl stretching/bending, and carbonate symmetry [43]. GO and rGO undergo hydroxyl, carboxylic, and carbonyl group elimination with heating, leading to exfoliation in 7 min [44].

3.3. X-ray Diffraction (XRD)

XRD uses the crystal diffraction of X-rays to study the crystalline structure, lattice parameters, phase analysis, and texture. The peak position reveals composition, while the intensity provides structural and phase information. [45]. The most common peak in graphite is $2\theta \sim 26.6^\circ$ [38], for GO it is $2\theta \sim 10.2^\circ$ [34,38,46–48], and for rGO it is $2\theta \sim 23^\circ$ [48]. Sharma et al. (2017) used XRD with a copper rotating anode and found that GO had a primary peak at (001) with a d-spacing of 1.45 nm, while rGO had a smaller d-spacing of 0.379 nm due to the removal of oxygen-containing functional groups. The large peak at

$2\theta = 19.6^\circ$ in rGO suggests incomplete oxidation (Figure 4a) [5]. In some results, graphite shows peaks at 50.68° (101), 54.62° (004), 59.84° (110), and 71.96° (112), indicating its crystalline structure. GO exhibits a sharp peak at 10.24° (002) with an interplanar distance of 0.80 nm [18,39]. An analysis of graphite, graphene oxide (GO), and reduced graphene oxide (rGO) shows graphite's strong peak at 26.62° and confirms its well-organized layered structure; GO showed a shifted peak at 9.03° , indicating complete oxidation and rGO had a wider peak at 24.10° , indicating restored conjugation (Figure 4b) [23]. GO also revealed turbostratic disorder with a peak $2\theta = 43^\circ$ [49]. XRD analysis of low GO shows a 002 reflection at 26.3° , suggesting a 12.9 nm thickness and 38 layers of the graphite-like structure [50]. For graphitic layers, coal shows peaks at 26.05° , 41.51° , and 55.97° (002, 101), respectively. Successful synthesis from coal is confirmed by the 14.26° (001) and 42.25° (100) peaks on the GO spectrum [51]. GO exhibits a peak at 10.57° and a wide range ($15\text{--}25^\circ$), corresponding to stacked GO nanosheets and graphite layers [52].

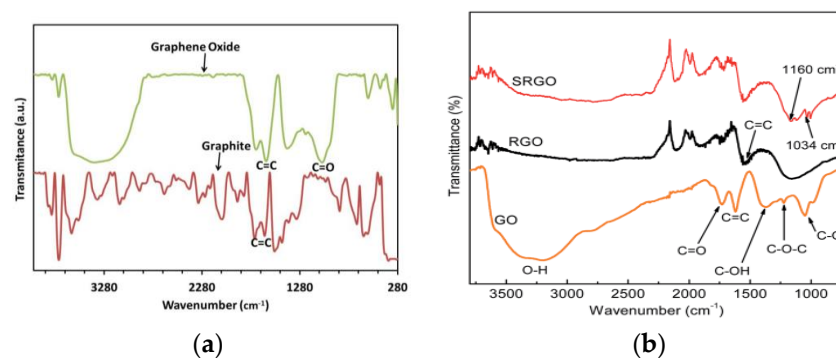


Figure 3. FTIR spectra of (a) graphite, GO; (b) GO, rGO, and sulfophenyl group modified rGO.

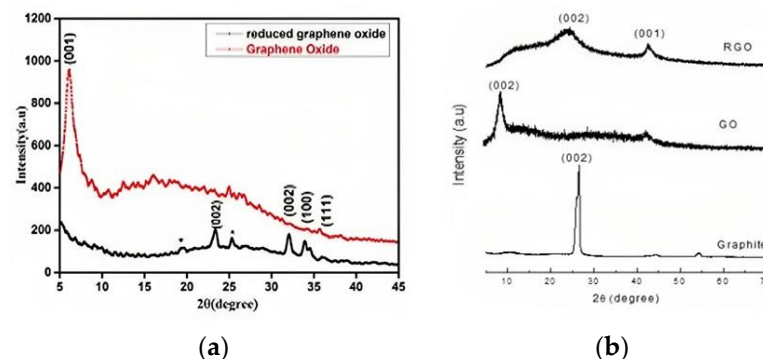


Figure 4. XRD pattern of (a) GO and rGO; (b) GO, rGO, graphite.

3.4. Atomic Force Microscope (AFM)

Krishnamoorthy et al. (2013) revealed the morphology of GO sample S-6 using AFM, depicting sheet-like structures with distinguishable single- and few-layered GO. (Figure 5). Clustering and self-assembly during drying caused multiple layers. Monolayers exhibited folds and high transparency, while wrinkles were observed in both monolayer and few-layered GO [38]. In tapping mode to image spray-coated materials on mica. Graphene oxide exhibited a layered morphology with a thickness of approximately 25 nm, containing embedded iron oxide particles of different sizes in samples S1 (70 nm) and S5 (200 nm) (Figure 6a–c) [53]. Treating a silicon substrate with drops of GO and rGO allowed them to dry for 30 min. The result was separate GO sheets (1.2 nm) and wrinkled, aggregated rGO sheets (1.05 nm), possibly due to exfoliation variations [54].

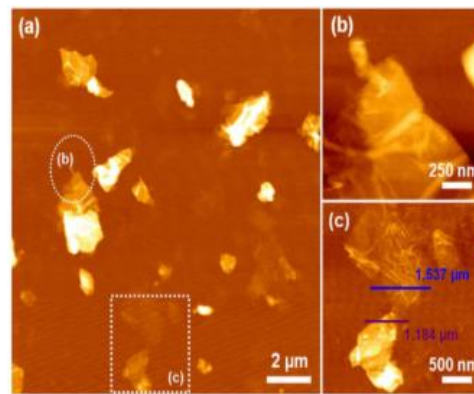


Figure 5. AFM image of (a) GO nanosheets; (b) enlarged circled area from (a); (c) enlarged squared area from (a).

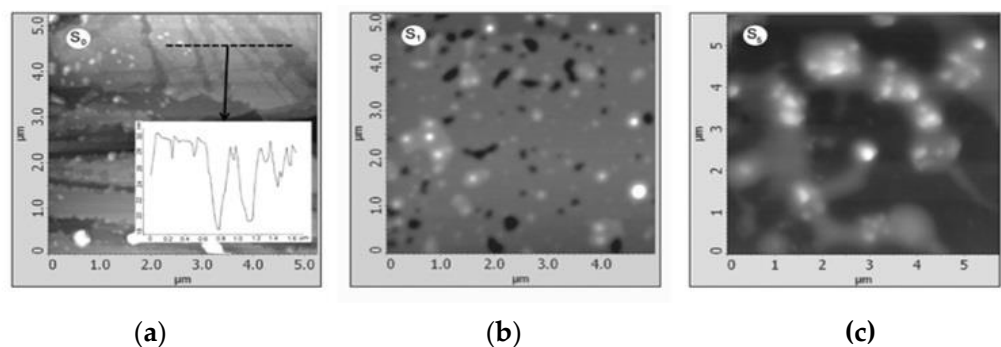


Figure 6. AFM images of (a) S_0 ; (b) S_1 ; (c) S_5 .

4. Mechanical Analysis

Babak, Fakhim, et al. (2014) analyzed the impact of varying amounts of graphene oxide (GO) on the tensile strength of cement mortar. The tensile strength increased with GO content to 1.5%, resulting in a 48% improvement compared to the control samples. However, beyond 1.5%, the tensile strength decreased [55]. The Young's modulus was determined by ultrasound, and hardness and fracture toughness were assessed with a Vickers Hardness Tester (98.1 N force, seven indentations). The result showed that there was a decrease in Young's modulus with increasing GO content correlated with relative densities. Due to the extreme sensitivity of the elastic modulus to porosity, pore shape, and agglomerates, even a slight reduction in relative density could result in a substantial drop in the elastic modulus [56].

Chen et al. (2012) investigated the tensile properties of GO and pure ultrahigh molecular weight polyethylene (UHMWPE) composites, which revealed that adding GO sheets increased the yield strength but decreased the ultimate tensile strength and elongation (Table 1) [57]. They found the optimal GO content to be 0.5 wt.%, while higher content led to decreased ductility and potential damage to UHMWPE chains. Strong GO-UHMWPE contact increased the yield strength, while a layered structure facilitated load transfer and energy absorption in composites with 0.5 wt.% GO. GO3 and GO4 in chitosan films enhanced tensile strength and Young's modulus, with maintained strength in wet conditions. Promising biomaterials [58]. GO/rGO enhances geopolymer flexural strength with increased dosage but decreases with excessive addition, negatively impacting mechanical strength [59].

Table 1. Mechanical characteristics of GO/UHMWPE composites with various GO contents.

Sample Description	Yield Strength (MPa)	Ultimate Tensile Strength (MPa)	Elongation at Break (%)
1% GO added in UHMWPE	23.38 ± 1.06	26.55 ± 0.80	1.53 ± 0.48
0.5% GO added in UHMWPE	23.70 ± 1.16	30.61 ± 1.72	2.76 ± 0.53
0.3% GO added in UHMWPE	23.42 ± 1.08	24.15 ± 1.56	1.20 ± 0.24
0.1% GO added in UHMWPE	23.03 ± 0.46	22.82 ± 0.76	0.88 ± 0.32
Pure UHMWPE	22.88 ± 0.77	30.45 ± 1.27	22.71 ± 0.47

5. Conclusions

Due to its exceptional qualities, graphene has received much attention in the field of material research. This review aimed to describe the various manufacturing processes and characteristics of GO and rGO. The exceptional qualities of graphene, its unique structure, and the simplicity with which GO and rGO can be functionalized all contribute to the amazing performances of these composites. There are still many problems to be solved before graphene can be used in practical applications though. For instance, producing graphene on a large scale with high quality and a homogeneous structure is still very difficult. Developing more eco-friendly and dependable technologies will make graphene-based systems and devices indispensable in our daily lives.

Author Contributions: Conceptualization, D.K.; methodology, P.V. and D.K.; software, P.V.; validation, D.K.; formal analysis, P.V.; investigation, P.V.; resources, P.V.; data curation, P.V.; writing—original draft preparation, P.V.; writing—review and editing, D.K. and S.K.; visualization, D.K. and S.K.; supervision, D.K.; project administration, D.K. and S.K. All authors have read and agreed to the published version of the manuscript.

Funding: This research received no external funding.

Institutional Review Board Statement: Not applicable.

Informed Consent Statement: Not applicable.

Data Availability Statement: Not applicable.

Conflicts of Interest: The authors declare no conflict of interest.

References

- Handayani, M.; Ganta, M.; Susilo, D.N.A.; Yahya, M.S.; Sunnardianto, G.K.; Darsono, N.; Sulistiyono, E.; Setiawan, I.; Lestari, F.P.; Erryani, A. Synthesis of graphene oxide from used electrode graphite with controlled oxidation process. *IOP Conf. Ser. Mater. Sci. Eng.* **2019**, *541*, 012032. [[CrossRef](#)]
- Jing, G.; Ye, Z.; Wu, J.; Wang, S.; Cheng, X.; Strokova, V.; Nelyubova, V. Introducing reduced graphene oxide to enhance the thermal properties of cement composites. *Cem. Concr. Compos.* **2020**, *109*, 103559. [[CrossRef](#)]
- Balandin, A.A.; Ghosh, S.; Bao, W.; Calizo, I.; Teweldebrhan, D.; Miao, F.; Lau, C.N. Superior thermal conductivity of single-layer graphene. *Nano Lett.* **2008**, *8*, 902–907. [[CrossRef](#)] [[PubMed](#)]
- Valentini, C.; Montes-García, V.; Livio, P.A.; Chudziak, T.; Raya, J.; Ciesielski, A.; Samorì, P. Tuning the electrical properties of graphene oxide through low-temperature thermal annealing. *Nanoscale* **2023**, *15*, 5743–5755. [[CrossRef](#)] [[PubMed](#)]
- Sharma, N.; Sharma, V.; Jain, Y.; Kumari, M.; Gupta, R.; Sharma, S.K.; Sachdev, K. Synthesis and characterization of graphene oxide (GO) and reduced graphene oxide (rGO) for gas sensing application. *Macromol. Symp.* **2017**, *376*, 1700006. [[CrossRef](#)]
- Karki, N.; Tiwari, H.; Tewari, C.; Rana, A.; Pandey, N.; Basak, S.; Sahoo, N.G. Functionalized graphene oxide as a vehicle for targeted drug delivery and bioimaging applications. *J. Mater. Chem. B* **2020**, *8*, 8116–8148. [[CrossRef](#)]
- Cho, E.S.; Ruminski, A.M.; Aloni, S.; Liu, Y.-S.; Guo, Y.-S.L.J.; Urban, J.J. Graphene oxide/metal nanocrystal multilaminates as the atomic limit for safe and selective hydrogen storage. *Nat. Commun.* **2016**, *7*, 10804. [[CrossRef](#)]
- Jiao, K.; Wang, X.; Wang, Y.; Chen, Y. Graphene oxide as an effective interfacial layer for enhanced graphene/silicon solar cell performance. *J. Mater. Chem. C* **2014**, *2*, 7715–7721. [[CrossRef](#)]
- Tshangana, C.S.; Muleja, A.A.; Kuvarega, A.T.; Malefetse, T.J.; Mamba, B.B. The applications of graphene oxide quantum dots in the removal of emerging pollutants in water: An overview. *J. Water Process. Eng.* **2021**, *43*, 102249. [[CrossRef](#)]
- Korucu, H.; Mohamed, A.I.; Yartaşı, A.; Uğur, M. The detailed Characterization of graphene oxide. *Chem. Pap.* **2023**, *77*, 5787–5806. [[CrossRef](#)]
- Zhou, A.; Yu, T.; Liang, X.; Yin, S. H₂O₂-free strategy derived from Hummers method for preparing graphene oxide with high oxidation degree. *FlatChem* **2023**, *38*, 100487. [[CrossRef](#)]

12. Acik, M.; Lee, G.; Mattevi, C.; Pirkle, A.; Wallace, R.M.; Chhowalla, M.; Cho, K.; Chabal, Y. The role of oxygen during thermal reduction of graphene oxide studied by infrared absorption spectroscopy. *J. Phys. Chem. C* **2011**, *115*, 19761–19781. [[CrossRef](#)]
13. Phiri, J.; Gane, P.; Maloney, T.C. General overview of graphene: Production, properties and application in polymer composites. *Mater. Sci. Eng. B* **2017**, *215*, 9–28. [[CrossRef](#)]
14. Surekha, G.; Krishnaiah, K.V.; Ravi, N.; Suvarna, R.P. FTIR, Raman and XRD analysis of graphene oxide films prepared by modified Hummers method. *J. Phys. Conf. Ser.* **2020**, *1495*, 012012. [[CrossRef](#)]
15. Pendolino, F.; Armata, N.; Pendolino, F.; Armata, N. Synthesis, characterization and models of graphene oxide. In *Graphene Oxide in Environmental Remediation Process*; Springer: Berlin/Heidelberg, Germany, 2017; pp. 5–21. [[CrossRef](#)]
16. Alghyamah, A.A.; Haider, S.; Khalil, U.; Khan, R.; Haider, A.; Almasry, W.A.; Ihsan, R.; Perveen, T.; Wazeer, I.; Chafidz, A. Synthesis and characterization of graphene oxide, reduced graphene oxide and their nanocomposites with polyethylene oxide. *Curr. Appl. Phys.* **2022**, *40*, 1–11. [[CrossRef](#)]
17. Rattana; Chaiyakun, S.; Witit-Anun, N.; Nuntawong, N.; Chindaudom, P.; Oaew, S.; Kedkeaw, C.; Limsuwan, P. Preparation and characterization of graphene oxide nanosheets. *Procedia Eng.* **2012**, *32*, 759–764. [[CrossRef](#)]
18. Ban, F.; Majid, S.; Huang, N.; Lim, H. Graphene Oxide and Its Electrochemical Performance. *Int. J. Electrochem. Sci.* **2012**, *7*, 4345–4351. [[CrossRef](#)]
19. Zhou, J.; Yao, Z.; Chen, Y.; Wei, D.; Wu, Y.; Xu, T. Mechanical and thermal properties of graphene oxide/phenolic resin composite. *Polym. Compos.* **2013**, *34*, 1245–1249. [[CrossRef](#)]
20. Lavin-Lopez, M.P.; Paton-Carrero, A.P.; Sanchez-Silva, L.; Valverde, J.L.; Romero, A. Influence of the reduction strategy in the synthesis of reduced graphene oxide. *Adv. Powder Technol.* **2017**, *28*, 3195–3203. [[CrossRef](#)]
21. Gautam, V.; Kumar, A.; Kumar, R.; Jain, V.K.; Nagpal, S. Silicon nanowires/reduced graphene oxide nanocomposite based novel sensor platform for detection of cyclohexane and formaldehyde. *Mater. Sci. Semicond. Process.* **2021**, *123*, 105571. [[CrossRef](#)]
22. Adetayo, A.; Runsewe, D. Synthesis and Fabrication of Graphene and Graphene Oxide: A Review. *Open J. Compos. Mater.* **2019**, *9*, 207–229. [[CrossRef](#)]
23. Hidayah, N.M.S.; Liu, W.-W.; Lai, C.-W.; Noriman, N.Z.; Khe, C.-S.; Hashim, U.; Lee, H.C. Comparison on graphite, graphene oxide and reduced graphene oxide: Synthesis and characterization. *AIP Conf. Proc.* **2017**, *1892*, 150002. [[CrossRef](#)]
24. Pathak, A.K.; Borah, M.; Gupta, A.; Yokozeki, T.; Dhakate, S.R. Improved mechanical properties of carbon fiber/graphene oxide-epoxy hybrid composites. *Compos. Sci. Technol.* **2016**, *135*, 28–38. [[CrossRef](#)]
25. Cheng-An, T.; Hao, Z.; Fang, W.; Hui, Z.; Xiaorong, Z.; Jianfang, W. Mechanical properties of graphene oxide/polyvinyl alcohol composite film. *Polym. Polym. Compos.* **2017**, *25*, 11–16. [[CrossRef](#)]
26. Chong, S.W.; Lai, C.W.; Hamid, S.B.A. Green preparation of reduced graphene oxide using a natural reducing agent. *Ceram. Int.* **2015**, *41*, 9505–9513. [[CrossRef](#)]
27. Buldu-Akturk, M.; Toufani, M.; Tufani, A.; Erdem, E. ZnO and reduced graphene oxide electrodes for all-in-one supercapacitor devices. *Nanoscale* **2022**, *14*, 3269–3278. [[CrossRef](#)]
28. Torrisi, L.; Silipigni, L.; Cutroneo, M.; Torrisi, A. Graphene oxide as a radiation sensitive material for XPS dosimetry. *Vacuum* **2020**, *173*, 109175. [[CrossRef](#)]
29. Pan, Z.; He, L.; Qiu, L.; Korayem, A.H.; Li, G.; Zhu, J.W.; Collins, F.; Li, D.; Duan, W.H.; Wang, M.C. Mechanical properties and microstructure of a graphene oxide–cement composite. *Cem. Concr. Compos.* **2015**, *58*, 140–147. [[CrossRef](#)]
30. Nasir, A.; Raza, A.; Tahir, M.; Yasin, T.; Nadeem, M.; Ahmad, B. Synthesis and study of polyaniline grafted graphene oxide nanohybrids. *Mater. Res. Bull.* **2023**, *157*, 112006. [[CrossRef](#)]
31. Cao, N.; Zhang, Y. Study of reduced graphene oxide preparation by hummers' method and related characterization. *J. Nanomater.* **2015**, *2015*, 168125. [[CrossRef](#)]
32. Gong, T.; Van Lam, D.; Liu, R.; Won, S.; Hwangbo, Y.; Kwon, S.; Kim, J.; Sun, K.; Kim, J.; Lee, S.; et al. Thickness dependence of the mechanical properties of free-standing graphene oxide papers. *Adv. Funct. Mater.* **2015**, *25*, 3756–3763. [[CrossRef](#)]
33. Koçanalı, A.; Varol, E.A. An experimental study on the electrical and thermal performance of reduced graphene oxide coated cotton fabric. *Int. J. Energy Res.* **2021**, *45*, 12915–12927. [[CrossRef](#)]
34. Muniyalakshmi, M.; Sethuraman, K.; Silambarasan, D. Synthesis and characterization of graphene oxide nanosheets. *Mater. Today Proc.* **2020**, *21*, 408–410. [[CrossRef](#)]
35. Song, J.; Wang, X.; Chang, C.-T. Preparation and characterization of graphene oxide. *J. Nanomater.* **2014**, *2014*, 276143. [[CrossRef](#)]
36. Tewatia, K.; Sharma, A.; Sharma, M.; Kumar, A. Synthesis of graphene oxide and its reduction by green reducing agent. *Mater. Today Proc.* **2021**, *44*, 3933–3938. [[CrossRef](#)]
37. Paulchamy, B.; Arthi, G.; Lignesh, B.D. A Simple approach to stepwise synthesis of graphene oxide nanomaterial. *J. Nanomed. Nanotechnol.* **2015**, *6*, 1. [[CrossRef](#)]
38. Krishnamoorthy, K.; Veerapandian, M.; Yun, K.; Kim, S.-J. The chemical and structural analysis of graphene oxide with different degrees of oxidation. *Carbon* **2013**, *53*, 38–49. [[CrossRef](#)]
39. Habte, A.T.; Ayele, D.W. Synthesis and characterization of reduced graphene oxide (rGO) started from graphene oxide (GO) using the tour method with different parameters. *Adv. Mater. Sci. Eng.* **2019**, *2019*, 5058163. [[CrossRef](#)]
40. Peng, H.; Ge, Y.; Cai, C.; Zhang, Y.; Liu, Z. Mechanical properties and microstructure of graphene oxide cement-based composites. *Constr. Build. Mater.* **2019**, *194*, 102–109. [[CrossRef](#)]

41. Ghorbani, M.; Abdizadeh, H.; Golobostanfard, M. Reduction of graphene oxide via modified hydrothermal method. *Procedia Mater. Sci.* **2015**, *11*, 326–330. [[CrossRef](#)]
42. Ossoonon, B.D.; Bélanger, D. Synthesis and characterization of sulfophenyl-functionalized reduced graphene oxide sheets. *RSC Adv.* **2017**, *7*, 27224–27234. [[CrossRef](#)]
43. Kakade, P.M.; Kachere, A.R.; Mandlik, N.T.; Rondiya, S.R.; Jadkar, S.R.; Bhosale, S.V. Graphene oxide assisted synthesis of magnesium oxide nanorods. *ES Mater. Manuf.* **2021**, *12*, 63–71. [[CrossRef](#)]
44. Sengupta, I.; Kumar, S.S.S.; Pal, S.K.; Chakraborty, S. Characterization of structural transformation of graphene oxide to reduced graphene oxide during thermal annealing. *J. Mater. Res.* **2020**, *35*, 1197–1204. [[CrossRef](#)]
45. Epp, J.; Huebschen, G.; Altpeter, I.; Tschuncky, R.; Herrmann, H.-G. X-ray diffraction techniques for material characterization. In *Materials Characterization Using Nondestructive Evaluation (NDE) Methods*; Woodhead Publishing: Sawston, UK, 2016; pp. 81–124. ISBN 978-0-08-100040-3. [[CrossRef](#)]
46. Yang, J.; Shojaei, S.; Shojaei, S. Removal of drug and dye from aqueous solutions by graphene oxide: Adsorption studies and chemometrics methods. *npj Clean Water* **2022**, *5*, 5. [[CrossRef](#)]
47. Guliyeva, N.A.; Abaszade, R.G.; Khanmammadova, E.A.; Azizov, E.M. Synthesis and analysis of nanostructured graphene oxide. *J. Optoelectron. Biomed. Mater.* **2023**, *15*, 23–30. [[CrossRef](#)]
48. Stobinski, L.; Lesiak, B.; Malolepszy, A.; Mazurkiewicz, M.; Mierzwa, B.; Zemek, J.; Jiricek, P.; Bieloshapka, I. Graphene oxide and reduced graphene oxide studied by the XRD, TEM and electron spectroscopy methods. *J. Electron Spectrosc. Relat. Phenom.* **2014**, *195*, 145–154. [[CrossRef](#)]
49. Emiru, T.F.; Ayele, D.W. Controlled synthesis, characterization and reduction of graphene oxide: A convenient method for large scale production. *Egypt. J. Basic Appl. Sci.* **2017**, *4*, 74–79. [[CrossRef](#)]
50. Abaszade, R.G. Synthesis and analysis of flakes graphene oxide. *J. Optoelectron. Biomed. Mater.* **2022**, *14*, 107–114. [[CrossRef](#)]
51. Sahoo, P.; Shubhadarshinee, L.; Jali, B.R.; Mohapatra, P.; Barick, A.K. Synthesis and characterization of graphene oxide and graphene from coal. *Mater. Today Proc.* **2022**, *56*, 2421–2427. [[CrossRef](#)]
52. Dan, S.; Bagheri, H.; Shahidizadeh, A.; Hashemipour, H. Performance of graphene Oxide/SiO₂ Nanocomposite-based: Antibacterial Activity, dye and heavy metal removal. *Arab. J. Chem.* **2023**, *16*, 104450. [[CrossRef](#)]
53. Singh, V.; Patra, M.; Manoth, M.; Gowd, G.; Vadera, S.; Kumar, N. In situ synthesis of graphene oxide and its composites with iron oxide. *New Carbon Mater.* **2009**, *24*, 147–152. [[CrossRef](#)]
54. Rathnayake, R.; Wijayasinghe, H.; Pitawala, H.; Yoshimura, M.; Huang, H.-H. Synthesis of graphene oxide and reduced graphene oxide by needle platy natural vein graphite. *Appl. Surf. Sci.* **2017**, *393*, 309–315. [[CrossRef](#)]
55. Babak, F.; Abolfazl, H.; Alimorad, R.; Parviz, G. Preparation and mechanical properties of graphene oxide: Cement nanocomposites. *Sci. World J.* **2014**, *2014*, 276323. [[CrossRef](#)] [[PubMed](#)]
56. Cygan, T.; Wozniak, J.; Kostecki, M.; Petrus, M.; Jastrzębska, A.; Ziemkowska, W.; Olszyna, A. Mechanical properties of graphene oxide reinforced alumina matrix composites. *Ceram. Int.* **2017**, *43*, 6180–6186. [[CrossRef](#)]
57. Chen, Y.; Qi, Y.; Tai, Z.; Yan, X.; Zhu, F.; Xue, Q. Preparation, mechanical properties and biocompatibility of graphene oxide/ultrahigh molecular weight polyethylene composites. *Eur. Polym. J.* **2012**, *48*, 1026–1033. [[CrossRef](#)]
58. Han, D.; Yan, L.; Chen, W.; Li, W. Preparation of chitosan/graphene oxide composite film with enhanced mechanical strength in the wet state. *Carbohydr. Polym.* **2011**, *83*, 653–658. [[CrossRef](#)]
59. Liu, X.; Wu, Y.; Li, M.; Jiang, J.; Guo, L.; Wang, W.; Zhang, W.; Zhang, Z.; Duan, P. Effects of graphene oxide on microstructure and mechanical properties of graphene oxide-geopolymer composites. *Constr. Build. Mater.* **2020**, *247*, 118544. [[CrossRef](#)]

Disclaimer/Publisher's Note: The statements, opinions and data contained in all publications are solely those of the individual author(s) and contributor(s) and not of MDPI and/or the editor(s). MDPI and/or the editor(s) disclaim responsibility for any injury to people or property resulting from any ideas, methods, instructions or products referred to in the content.